Title

On the Fe K absorption – accretion state connection in the Galactic Centre neutron star X-ray binary AX J1745.6-2901

Authors

Ponti, G
Bianchi, S
Muñoz-Darias, T
et al.

On the Fe K absorption – accretion state connection in the Galactic Centre neutron star X-ray binary AX J1745.6-2901

G. Ponti,[1]⋆ S. Bianchi,[2] T. Muñoz-Darias,[3] B. De Marco,[1] T. Dwelly,[1] R. P. Fender,[3] K. Nandra,[1] N. Rea,[4,5] K. Mori,[6] D. Haggard,[7] C. O. Heinke,[8] N. Degenaar,[9] T. Aramaki,[6] M. Clavel,[10,11] A. Goldwurm,[10,11] C. J. Hailey,[6] G. L. Israel,[12] M. R. Morris,[13] A. Rushton[3,14] and R. Terrier[10]

[1] *Max-Planck-Institut für Extraterrestrische Physik, Giessenbachstrasse, D-85748 Garching, Germany*
[2] *Dipartimento di Matematica e Fisica, Università Roma Tre, Via della Vasca Navale 84, I-00146 Roma, Italy*
[3] *Astrophysics, Department of Physics, University of Oxford, Denys Wilkinson Building, Keble Road, Oxford OX1 3RH, UK*
[4] *Astronomical Institute Anton Pannekoek, University of Amsterdam, Postbus 94249, NL-1090 GE Amsterdam, the Netherlands*
[5] *Institute of Space Sciences (CSIC-IEEC), Campus UAB, Torre C5, 2a planta, E-08193 Barcelona, Spain*
[6] *Columbia Astrophysics Laboratory, Columbia University, New York, NY 10027, USA*
[7] *CIERA and Physics and Astronomy Department, Northwestern University, 2145 Sheridan Road, Evanston, IL 60208, USA*
[8] *Department of Physics, University of Alberta, CCIS 4-183, Edmonton, AB T6G 2E1, Canada*
[9] *Department of Astronomy, University of Michigan, 500 Church Street, Ann Arbor, MI 48109, USA*
[10] *AstroParticule et Cosmologie, Université Paris Diderot, CNRS/IN2P3, CEA/DSM, Observatoire de Paris, Sorbonne Paris Cité,*
10 rue Alice Domon et Léonie Duquet, F-75205 Paris Cedex 13, France
[11] *Service d' Astrophysique/IRFU/DSM, CEA Saclay, Bât. 709, F-91191 Gif-sur-Yvette Cedex, France*
[12] *INAF – Osservatorio astronomico di Roma, Via Frascati 44, I-00040 Monteporzio Catone (Roma), Italy*
[13] *Department of Physics & Astronomy, University of Calisfornia, Los Angeles, CA 90095-1547, USA*
[14] *School of Physics and Astronomy, University of Southampton, Highfield, Southampton SO17 1BJ, UK*

ABSTRACT

AX J1745.6-2901 is a high-inclination (eclipsing) neutron star low-mass X-ray binary (LMXB) located less than ∼1.5 arcmin from Sgr A⋆. Ongoing monitoring campaigns have targeted Sgr A⋆ frequently and these observations also cover AX J1745.6-2901. We present here an X-ray analysis of AX J1745.6-2901 using a large data set of 38 *XMM–Newton* observations, including 11 which caught AX J1745.6-2901 in outburst. Fe K absorption is clearly seen when AX J1745.6-2901 is in the soft state, but disappears during the hard state. The variability of these absorption features does not appear to be due to changes in the ionizing continuum. The small Kα/Kβ ratio of the equivalent widths of the Fe XXV and Fe XXVI lines suggests that the column densities and turbulent velocities of the absorbing ionized plasma are in excess of $N_{\mathrm{H}} \simeq 10^{23}$ cm^{-2} and $v_{\mathrm{turb}} \gtrsim 500$ km s^{-1}. These findings strongly support a connection between the wind (Fe K absorber) and the accretion state of the binary. These results reveal strong similarities between AX J1745.6-2901 and the eclipsing neutron star LMXB, EXO 0748-676, as well as with high-inclination black hole binaries, where winds (traced by the same Fe K absorption features) are observed only during the accretion-disc-dominated soft states, and disappear during the hard states characterized by jet emission.

Key words: accretion, accretion discs – black hole physics – stars: neutron – stars: winds, outflows – X-rays: binaries – X-rays: individual: AX J1745.6-2901.

1 INTRODUCTION

Equatorial accretion disc winds have recently been demonstrated to be a ubiquitous feature of accreting black holes (BHs; Ponti et al. 2012a). Such winds have almost always been observed during the soft state and typically disappear during the canonical hard state

⋆ E-mail: ponti@iasfbo.inaf.it

(Neilsen & Lee 2009; Miller et al. 2012; Ponti et al. 2012). The estimated wind mass outflow rates (Lee et al. 2002; Ueda et al. 2004; Miller et al. 2006; Neilsen, Remillard & Lee 2011; King et al. 2012; Ponti et al. 2012) and their tight connection with the accretion state suggest that winds are a fundamental component of the accretion process in BH binaries.

Accreting neutron stars (NS) are also known to have equatorial absorbers and winds (Sidoli et al. 2001; Ueda et al. 2001; Parmar et al. 2002; Boirin & Parmar 2003; Boirin et al., 2004, 2005;

Díaz-Trigo et al. 2006; Díaz-Trigo & Boirin 2013, but see also Miller et al. 2011); however, a one-to-one connection between the wind and accretion state is still to be established. A recent study focused on the absorption properties of the NS low-mass X-ray binary (LMXB) EXO 0748-676 (Ponti, Muñoz-Darias & Fender 2014). This source has been continuously in outburst for 23 years (it was discovered in 1985 and it returned to quiescence in 2008; Parmar et al. 1985; Hynes & Jones 2008; Wolff et al. 2008). As characteristic of the high-inclination sources, EXO 0748-676 shows dips and eclipses. An inclination of $75 < i < 83°$ was estimated (Parmar et al. 1985, 1986) for a primary mass of $M_{NS} \sim 1.4\, M_{\odot}$, which is consistent with dynamical estimates (Muñoz-Darias, Motta & Belloni 2011; Ratti et al. 2012). No Fe K absorption lines are detected during the more than 20 *XMM–Newton* observations which catch EXO 0748-676 in the hard state. None the less, intense Fe XXIII, Fe XXV and Fe XXVI absorption lines are clearly observed in the single *XMM–Newton* observation where EXO 0748-676 is seen in the soft state (Ponti et al. 2014). This suggests that the wind–accretion state connection might also be present in some accreting NS binaries. To further test this hypothesis, we analyse the *XMM–Newton* and *Swift* observations (as well as *NuSTAR* data to constrain the broad-band spectral energy distribution; SED) of another well-known high-inclination (dipping and eclipsing) accreting NS, AX J1745.6-2901.

At less than 1.5 arcmin from Sgr A⋆, AX J1745.6-2901 lies within one of the most intensely observed patches of the X-ray sky. AX J1745.6-2901 was identified as a new transient X-ray burster near the Galactic Centre in 1993–1994 and 1997 *ASCA* observations (Kennea & Skinner 1996; Maeda et al. 1996; Sakano et al. 2002). Intensity dips with a period of 8.356 ± 0.008 h were identified, indicating the high inclination of the source. Excess soft X-rays during the dips are attributed to scattering by interstellar dust (Maeda et al. 1996).

Muno et al. (2003) catalogued a faint ($L_X \sim 10^{32}$ erg s^{-1}, for an 8 kpc distance) *Chandra* X-ray source, CXOGC J174535.6-290133, confirmed to be the quiescent X-ray counterpart of AX J1745.6-2901 (Heinke et al. 2008). New transient outbursts were seen by *Swift*, *INTEGRAL*, *XMM–Newton*, *Chandra* and *Suzaku* in early 2006 (Chenevez et al. 2006; Kennea et al. 2006), in 2007–2008 (Porquet et al. 2007; Wijnands et al. 2007; Degenaar & Wijnands 2009, 2010a; Hyodo et al. 2009;), in 2010 (Degenaar et al. 2010b) and 2013–2014 (Degenaar et al. 2013b, 2014a). The 2006 and 2010 outbursts were short (4 and 4–7 months, respectively[1]) and low luminosity (peak $L_X \sim 5 \times 10^{35}$ erg s^{-1}), while the 2007–2008 and 2013–2014 outbursts were longer (1.5–1.7 and >1 yr to date) and of higher luminosity (peak $L_{2-10\,keV} \sim 7 \times 10^{36}$ erg s^{-1} for both; Degenaar & Wijnands 2010a; Degenaar et al. 2014a).

As observed in many other high-inclination systems (e.g. Boirin et al. 2004; Díaz-Trigo et al. 2006, Díaz-Trigo et al. 2013), AX J1745.6-2901 shows eclipses, dips and Fe K absorption (both Fe XXV and Fe XXVI Kα and Kβ absorption; Hyodo et al. 2009). The observed equivalent widths of these absorption lines range from $\sim$30 to 60 eV, and the lines are observed during all orbital phases (except eclipses). Therefore, a disc corona origin for the absorbing material has been proposed (Hyodo et al. 2009). Hyodo et al. (2009) suggested that the absorbing gas is outflowing with a bulk motion of $\sim$10^3 km s^{-1}, and also showed that the dip spectra are well re-

produced by increased absorption by cold (approximately neutral) material.

A total of 38 *XMM–Newton* observations included AX J1745.6-2901, of which 11 have caught the source in outburst. The detailed *Swift* monitoring of the Galactic Centre (Degenaar & Wijnands 2009, 2010a, Degenaar et al. 2013a, 2014b), comprising over 1000 *Swift* snapshot observations obtained between 2006 and 2014, allows us to place the *XMM–Newton* observations in context, tracking the accretion state of AX J1745.6-2901. Taken together, these data provide us with a unique opportunity to study the wind in AX J1745.6-2901 and determine whether the appearance/disappearance of the wind is linked to the accretion state of the source.

The paper is organized as follows. In Section 2, we present the *XMM–Newton* and *Swift* observations and data reduction methods. In Section 3, we present the method used to determine the accretion state. In Sections 4 and 5, we present detailed modelling of the *XMM–Newton* data using phenomenological and proper photoionization models. Our results are summarized in Section 6.

2 OBSERVATIONS AND DATA REDUCTION

All spectral fits were performed using the XSPEC software package (version 12.7.0). Uncertainties and upper limits are reported at the 90 per cent confidence level for one interesting parameter, unless otherwise stated. The reported X-ray fluxes are not corrected for Galactic absorption. To allow the use of χ^2 statistics, we group each spectrum to have a minimum of 25 counts in each bin. We adopt a nominal Eddington limit for AX J1745.6-2901 of $L_{Edd} = 2 \times 10^{38}$ erg s^{-1} (appropriate for a primary mass of $M_{NS} \sim 1.4\, M_{\odot}$ and cosmic composition; Lewin, van Paradijs & Taam 1993).

2.1 *XMM–Newton*

Several independent groups with a wide variety of science goals have made *XMM–Newton* observations of the Galactic Centre field over the last decade. In this paper, we combine all available data where AX J1745.6-2901 lies within the *XMM–Newton* field of view. This includes recent *XMM–Newton* observations which were designed to monitor the passage of G2 (Gillessen et al. 2012) at pericentre (PIs: Haggard; Ponti), and to track the evolution of the outburst of SGR J1745-2900 (Kennea et al. 2013; Mori et al. 2013; Rea et al. 2013; PI: Israel), data from the *XMM–Newton* scan of the central molecular zone (PI: Terrier), plus many older archival *XMM–Newton* observations (see Table 1, and tables 3 and 5 of Ponti et al. in preparation).

As of 2014 May 14, there were 34 observations publicly available in the *XMM–Newton* archive (Table 1), pointed near AX J1745.6-2901 and with EPIC-pn clean exposure longer than 3 ks. We add to this four new proprietary observations that were accumulated between 2013 August and 2014 April.

Starting from the *XMM–Newton* observation data files, we reprocess all the data sets, with the latest version (13.5.0) of the *XMM–Newton* Science Analysis System (SAS), applying the most recent (as of 2014 May 14) calibrations. Because of the relatively small effective area of the MOS cameras in the Fe *K* band, we restrict our analysis here to data collected with the EPIC-pn camera.

The majority of the EPIC-pn observations have been accumulated in Full Frame mode with the medium filter. One observation (OBSID 0112972101) was performed in Extended Full Frame mode, and two (OBSIDS 0111350301 and 0111350101) used the thick filter.

Photon pile-up affected all observations in which AX J1745.6-2901 was found in the soft state (see Section 3; Table 1). To mitigate

---

[1] The end date of the 2010 outburst is uncertain as it occurred when AX J1745.6-2901 was too close to the Sun to be monitored by *Swift* or any other X-ray Telescope (XRT).

Table 1. A list of all *XMM–Newton* observations considered in this work. The columns of the table report the *XMM–Newton* OBSID, the *XMM–Newton* revolution, the observation start date and time, the observation duration and the EPIC-pn exposure time after cleaning, the source state (H = hard state; S = soft state; D = detected (the source is detected but is still in quiescence); Q = quiescent). The following columns give the 3–6, 6–10 and 8–10 keV observed (absorbed) fluxes in units of 10^{-12} erg cm^{-2} s^{-1}. ♭ The fluxes of AX J1745.6-2901 during the observations in quiescence are $F_{3-6\,keV} < 5 \times 10^{-14}$ and $F_{6-10\,keV} < 8 \times 10^{-14}$ erg cm^{-2} s^{-1}. The last column shows, in order, the count rate thresholds applied to select bursting, eclipsing and intense dipping periods, the hard and soft count rates and the threshold to select out intense particle activity periods. A more exhaustive description of the data reduction and cleaning is provided in Section 2.1. ¶ Data sets used to compute the source background for the outburst observations. ‡Exposure too short to compute a meaningful upper limit on the flux of AX J1745.6-2901 (no source emission is observed even in the uncleaned data).

XMM–Newton OBSID	Rev	Start (UTC)	Exp (ks)	CL Exp (ks)	State	F_{3-6}	F_{6-10} (10^{-12} erg cm^{-2} s^{-1})	F_{8-10}	Threshold (ct s^{-1})
0690441801	2622	2014-04-03 05:06:00	86.5	69.1	H	5.95	10.1	4.75	3.5/0.24/1.5/0.65/0.5/1.5
0724210501	2525	2013-09-22 21:15:49	43.9	30.0	S	55.8	59.8	21.7	10/1.1/1.4/5/3.8/1.5
0700980101	2519	2013-09-10 03:30:45	38.7	30.6	S	78.3	91.5	33.5	13/1.5/1.4/7/5/1.5
0724210201	2514	2013-08-30 20:13:12	58.5	45.7	S	72.9	91.5	34.5	13/1.6/1.5/7/4.5/1.4
0694641101	2343	2012-09-24 10:16:44	41.9	35.6	Q	♭	♭		0.8
0694641001	2343	2012-09-23 20:20:07	47.9	40.8	Q	♭	♭		0.85
0694640301	2331	2012-08-31 11:20:26	41.9	35.5	Q	♭	♭		0.75
0674601001	2249	2012-03-21 03:30:40	23.9¶	17.2	Q	♭	♭		0.7
0674600801	2248	2012-03-19 03:52:38	22.9¶	15.0	Q	♭	♭		0.7
0674601101	2247	2012-03-17 02:30:16	28.0¶	9.8	Q	♭	♭		0.6
0674600701	2246	2012-03-15 04:47:06	15.9	0.1‡	Q				0.8
0674600601	2245	2012-03-13 03:52:36	21.5¶	7.4	Q	♭	♭		0.9
0658600201	2148	2011-09-01 20:03:48	53.2¶	36.5	Q	♭	♭		0.9
0658600101	2148	2011-08-31 23:14:23	49.9¶	41.9	Q	♭	♭		0.9
0604301001	2073	2011-04-05 07:09:33	50.7¶	28.7	Q	♭	♭		0.6
0604300901	2072	2011-04-03 07:52:07	46.9¶	16.8	Q	♭	♭		0.6
0604300801	2071	2011-04-01 07:48:13	48.8¶	29.5	Q	♭	♭		0.7
0604300701	2070	2011-03-30 07:44:39	48.9¶	28.5	Q	♭	♭		0.6
0604300601	2069	2011-03-28 07:49:58	48.8¶	24.9	Q	♭	♭		0.6
0554750601	1707	2009-04-05 02:17:13	39.1¶	27.3	Q	♭	♭		0.6
0554750501	1706	2009-04-03 01:33:27	44.3¶	33.4	Q	♭	♭		0.65
0554750401	1705	2009-04-01 00:55:25	39.9¶	27.5	Q	♭	♭		0.65
0511000401	1610	2008-09-23 15:15:50	6.9	4.4	D	0.15	0.23	0.10	
0505670101	1518	2008-03-23 14:59:43	105.7	65.2	S	64.6	75.7	27.9	11/1.3/1.3/5/4/1.6
0511000301	1508	2008-03-03 23:25:56	6.9	4.4	S	72.4	85.0	31.1	12/1.5/1.4/5/3.7/20
0504940201	1418	2007-09-06 10:05:50	13.0	8.5	S	54.7	60.5	22.2	12/1.2/1.5/4.2/3.2/2.5
0402430401	1340	2007-04-03 14:32:24	105.7	38.6	S	74.9	95.6	36.4	12/1.5/1.4/6/4.3/1.5
0402430301	1339	2007-04-01 14:45:02	105.4	59.6	S	78.2	99.0	37.9	12/1.4/1.3/6/5/2
0402430701	1338	2007-03-30 21:05:17	34.2	24.4	S	84.6	105	39.8	12/1.5/1.4/6/4.3/2
0302884001	1236	2006-09-08 16:56:48	6.9	3.4	D	0.37	0.68	0.33	2/0/1.1/0.08/0.07/0.6
0302882601	1139	2006-02-27 04:04:34	6.9	4.0	H	8.02	13.7	6.28	4/0.001/1.2/0.9/0.6/5
0202670801	867	2004-09-02 03:01:39	135.2	75.2	D	0.21	0.38	0.18	0.65
0202670701	866	2004-08-31 03:12:01	135.2	81.8	D	0.20	0.28	0.12	0.6
0202670601	789	2004-03-30 14:46:36	134.4	27.2	D	0.37	0.68	0.33	0.6
0202670501	788	2004-03-28 15:03:52	133.0	13.7	D	0.23	0.44	0.22	0.6
0111350301	516	2002-10-03 06:54:11	17.3	7.6	D	0.44	0.87	0.43	0.55
0111350101	406	2002-02-26 03:16:43	52.8	35.8	D	0.11	0.19	0.09	0.6
0112972101	318	2001-09-04 01:20:42	26.7	18.2	Q	♭	♭		0.55

the effects of pile-up on the extracted spectra in the soft state, we adopt an annular extraction region centred on the source, with inner radius of $r_{in} = 9.25$ arcsec and outer radius of $r_{out} = 45$ arcsec (see e.g. van Peet et al. 2009). Discarding all the photons within 9.25 arcsec of the peak of the source point spread function, we remove ∼50 per cent of the encircled energy from the source which is concentrated on a small area (see fig. 7 in section 3.2.1.1 of the *XMM–Newton* users' handbook[2]). This allows us to reduce the

effects of pile-up significantly. An outer radius of 45 arcsec allows us to retain ∼95 per cent of the remaining source photons, whilst keeping the instrumental background and diffuse emission low. For the hard-state observations, which are not affected by pile-up, we extracted events using a circular region with 45 arcsec radius. To compute the source flux during the quiescent (or close to quiescence) observations whilst minimizing the contamination from instrumental background and diffuse emission, we used a small circular extraction region with a radius of 10 arcsec (see Table 1).

We initially selected the background photons from a region of similar size and shape and on the same detector chip as the source region. However, due to the bright and highly inhomogeneously

[2] http://xmm.esac.esa.int/external/xmm_user_support/documentation/uhb/index.html

distributed diffuse emission near the Galactic Centre (Wang, Gotthelf & Lang 2002; Baganoff et al. 2003; Koyama et al. 2007; Ponti et al. 2010, 2013; Clavel et al. 2013), we decided to accumulate the background spectrum from the same region of the sky selected for the source during the *XMM–Newton* observations where AX J1745.6-2901 was in quiescence (see Table 1). To mitigate the effects of the spatial and long-term temporal dependence of the internal EPIC-pn particle background, we selected only the quiescent state observations in which AX J1745.6-2901 was near the optical axis of the EPIC-pn instrument and which were taken after 2006 September (corresponding to the first observation in which AX J1745.6-2901 was observed in outburst by *XMM–Newton*, see Table 1). We identified periods of enhanced particle-induced background activity by calculating the full detector light curve in the 12–15 keV band, after excluding the events within a 2.5 arcmin radius of AX J1745.6-2901. Excluding all photons within 2.5 arcmin from the source ensures that more than 95 per cent of the photons from AX J1745.6-2901 are removed and that the emission from Sgr A⋆ and its immediate surrounding are also excluded. Time intervals with a count rate higher than the threshold specified in Table 1 were filtered out and not considered in further analysis.

In order to identify and remove type I bursts from the analysis, we used a 3 s resolution hard-band X-ray light curve. The 5–10 keV band was chosen for this as it is only marginally affected by dipping (Díaz-Trigo et al. 2006; van Peet et al. 2009; Ponti et al. 2014). We identified the intervals where AX J1745.6-2901 was in eclipse using a 60 s binned 5–10 keV light curve. The thresholds we applied are reported in Table 1.

Absorption dips are generally revealed by sudden increases in the hardness ratio. Therefore, to investigate the dipping phenomenon, we examined the hardness-ratio light curve, defined here as the ratio of the 5–10 keV light curve to the 0.5–5 keV light curve. Following van Peet et al. (2009) and Ponti et al. (2014), we determined the average hardness ratio for those intervals clearly belonging to the persistent emission, and then flagged as *dipping* those periods having hardness ratio 1.5 times larger than the persistent value. We note that the light curves of the source are only moderately affected by the dipping phenomenon. However, this might be due to the high foreground absorption column density towards AX J1745.6-2901, which prevents us from directly studying the soft X-ray energies where dips are most easily revealed.

After applying the particle background cut and the removal of bursts and eclipses, we extracted, for each observation, a source spectrum of the persistent emission plus mild dipping (e.g. dips with hardness ratio lower than 1.5 time quiescence; see Table 1 and Ponti et al. 2014). For each spectrum, the response matrix and effective area have been computed with the XMM-SAS tasks RMFGEN and ARFGEN.

2.2 *NuSTAR*

Several *NuSTAR* observations of the Sgr A⋆ field have been carried out to date, with the primary science goal of monitoring the time evolution of the newly discovered magnetar SGR J1745-29 (Kaspi et al. 2014). Four of these observations caught AX J1745.6-2901 during its 2013 outburst (which began on 2013 July 25). These four observations were carried out on 2013 July 31, August 8, 9 and 13, and have exposure times 22.3, 12.0, 11.2 and 11.7 ks, respectively (*NuSTAR* OBSIDs 80002013018, 80002013020, 80002013022 and 80002013024). No further *NuSTAR* observations of the Galactic Centre were performed until 2014 June. In each of the four *NuSTAR* observations, AX J1745.6-2901 was the brightest source in the

field of view, yielding adequate photon statistics to study spectral evolution over time. In this paper, *NuSTAR* data were used only to constrain the hardest and softest broad-band SED exhibited by AX J1745.6-2901. Full details of the outburst evolution and an analysis of type-I X-ray bursts will be presented by Hailey et al. (in preparation), but here we briefly describe our *NuSTAR* data analysis.

All *NuSTAR* data processing was performed with the *NuSTAR* Data Analysis Software (NUSTARDAS) v.1.3.1. *NuSTAR* consists of two co-aligned XRT (FPMA and FPMB) with an energy range 3–79 keV and having spectral resolution 400 eV (FWHM) at 10 keV (Harrison et al. 2013). We first filtered out time intervals containing type-I X-ray bursts in a similar way to that carried out for the *XMM–Newton* data, then extracted source photons from a 30 arcsec radius circle around the source position of AX J1745.6-2901. This extraction region is well calibrated for a point source, and results in negligible contamination from the nearby magnetar SGR J1745-29 (~1.5 arcmin away from AX J1745.6-2901). We extracted background spectra from a pre-outburst *NuSTAR* observation taken on 2013 July 7 (OBSID 8002013016, i.e. the last observation before the outburst) using the source extraction region. We re-binned the *NuSTAR* spectra to minimum 30 counts per bin, and discarded events outside the nominal *NuSTAR* bandpass (3–79 keV). We found that the softest and hardest spectra of AX J1745.6-2901 were observed in OBSIDs 80002013018 and 80002013024, respectively. We fit the softest observation (FPMA and FPMB spectra jointly) using the XSPEC model `phabs*simpl*diskbb` (see Steiner et al. 2009 for more details about the SIMPL Comptonization component). We use the same model to fit the hard-state observation even if the peak of the disc blackbody component is not in the *NuSTAR* band (see Section 5.2). The fit parameters were later adopted to construct the input SED data for our photoionization models (Section 5).

2.3 *Swift*

The *Swift* telescope has been used to regularly monitor the Galactic Centre field since 2006 February, typically making one or more short (~1 ks) snapshot observations on each day when the Galactic Centre is visible (Degenaar et al. 2013a). Our reduction of the *Swift*–XRT (Burrows et al. 2000) data utilizes a pipeline developed for monitoring campaigns of bright AGN (see Cameron et al. 2012; Fabian et al. 2012; Connolly, McHardy & Dwelly 2014). We have extracted an X-ray light curve for AX J1745.6-2901 using all *Swift*–XRT 'photon counting' mode observations with a nominal aim point within 25 arcmin of Sgr A⋆. For the work presented in this paper, we have analysed a total of 1116 *Swift* OBSIDs, including over 2000 separate visits with a summed exposure time of 1226 ks.

The raw *Swift*–XRT data sets were downloaded from the HEASARC archive and reprocessed using the tool XRTPIPELINE (version 0.12.8). For each *Swift* visit, we used XSELECT to extract source events from a 30 arcsec radius circular aperture centred on 17:45:35.65, −29:01:34.0 (J2000). Background events were extracted from a nearby 60 arcsec radius circular region containing no bright sources (centre 17:45:28.90, −29:03:44.2, J2000). We measured the number of detected counts in the source and background regions for each of a standard set of 10 medium-width energy bands spanning the range 0.3–10 keV. The background-subtracted source count rate in each energy band was calculated from the observed counts taking account of the relative sky areas of the source and background regions.

The sensitivity of *Swift*–XRT varies across the focal plane due to vignetting and the presence of bad pixels. We have compensated for the varying instrumental sensitivity between visits by
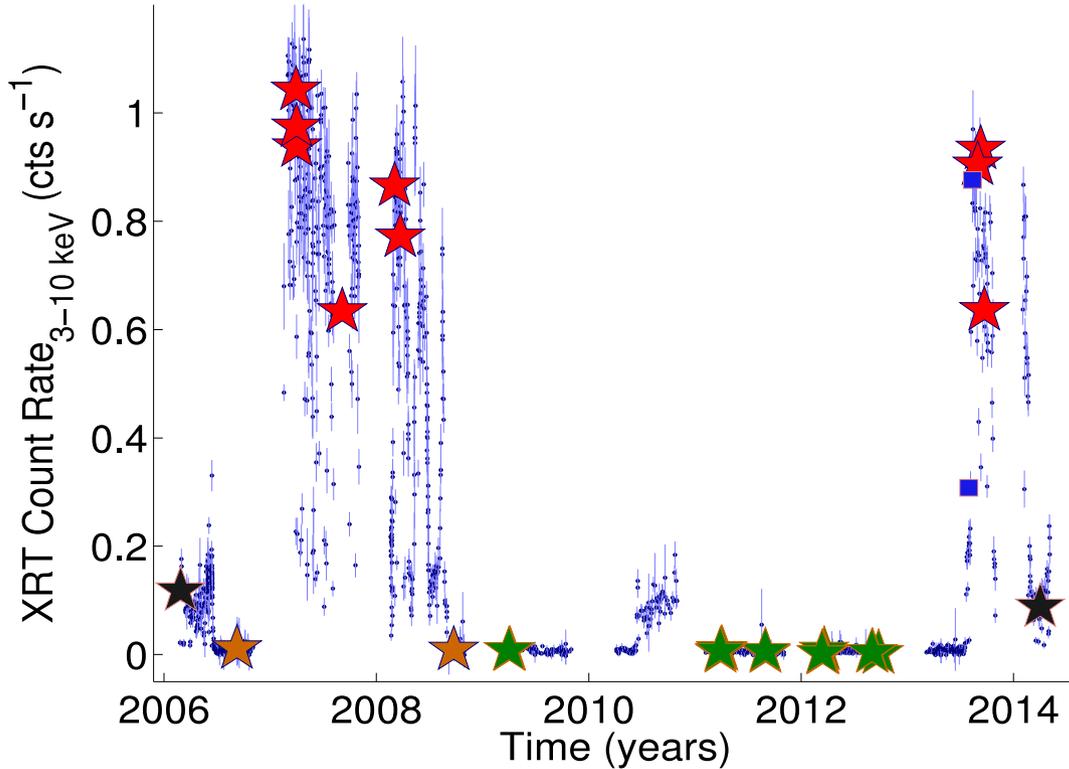
Figure 1. The X-ray light curve of AX J1745.6-2901, spanning >8 yr of *Swift*, *XMM–Newton* and *NuSTAR* observations. Each small blue point shows the normalized 3–10 keV count rate for each *Swift* visit. The large stars indicate the *XMM–Newton* EPIC-pn count rate (converted to the equivalent *Swift*–XRT count rate) measured during the observations which caught AX J1745.6-2901 in the quiescent (green/light-grey), hard (black) and soft (red/dark-grey) states. The blue squares indicate the observed count rate (converted to the equivalent *Swift*–XRT count rate) during the hardest and softest *NuSTAR* observations, which were used to constrain the source's broad-band SED (see Section 5.2). The *XMM–Newton* observations before 2006 all found AX J1745.6-2901 in the quiescent state and so are not shown.

calculating visit-specific corrections using the following method. For each visit, we generated an ARF file using the standard *Swift* tools (XRTEXPOMAP and XRTMKARF). Using this visit-specific ARF, the nominal XRT response matrix, a simple absorbed power-law spectral model and the FAKEIT function within XSPEC, we calculated the expected count rate for the visit-specific source extraction aperture ($R_{fake, i}$) and the count rate expected using the nominal *Swift*–XRT effective area curve and an infinite radius aperture ($R_{fake, 0}$). The count rate measured in the ith visit, R_i, can then be detrended using the following relation $R_{corrected, i} = R_i (R_{fake, 0}/R_{fake, i})$. We assumed a simple spectral model consisting of a power-law slope of $\Gamma = 1.9$ and Galactic $N_H = 1.2 \times 10^{22}$ cm^{-2}, but note that the detrending method is only weakly dependent on spectral shape due to our use of medium-width energy bands.

The detrended count rate in the 3–10 keV energy band was calculated by summing the detrended count rates calculated for the 3–4, 4–5, 5–6, 6–7 and 7–10 keV bands. Uncertainties were calculated by summing in quadrature the uncertainties in each band.

In a number of visits, the source position was located close to one or more of the bad columns on the *Swift*–XRT CCD; these data points have very uncertain correction factors and so are rejected from further consideration. Note that the *Swift*–XRT observations are expected to suffer from moderate pile-up effects when AX J1745.6-2901 is in its highest luminosity state. However, as we do not carry out a spectral analysis of the *Swift*–XRT data, we do not attempt to correct for pile-up in this work.

3 ACCRETION STATE DETERMINATION

Fig. 1 shows the long-term 3–10 keV light curve of AX J1745.6-2901 as measured by *Swift*–XRT. The locations and equivalent count rates for all *XMM–Newton* observations plus those for the hardest and softest *NuSTAR* observations are also indicated.[3] During 11/38 *XMM–Newton* observations, AX J1745.6-2901 was caught in outburst, with $F_{3-10\,keV} \geq 1.6 \times 10^{-11}$ erg cm^{-2} s^{-1}. AX J1745.6-2901 was in quiescence during 19/38 *XMM–Newton* observations, i.e. it was undetected in the 3–10 keV band, implying a luminosity lower than $\sim 9 \times 10^{32}$ erg s^{-1} (assuming a distance of 8 kpc). During the remaining 8/38 observations, AX J1745.6-2901 was detected (see Table 1) at a slightly higher flux of $F_{3-10\,keV} \leq 1.3 \times 10^{-12}$ erg cm^{-2} s^{-1} corresponding to luminosities of $L_{3-10\,keV} \leq 10^{34}$ erg s^{-1}, and Eddington ratios of $L_{3-10\,keV}/L_{Edd} \leq 5 \times 10^{-5}$; therefore, although detected, it has still been caught in the quiescent state.

The observed high column density of neutral material ($N_H \sim 1.9 \times 10^{23}$ cm^{-2}) suggests that AX J1745.6-2901 is located at or behind the Galactic Centre (see Section 4.1). The distance of AX J1745.6-2901 along the line of sight is uncertain. If located at a

---

[3] We first derive the 3–10 keV flux from the best-fitting model (see Section 4) for each of the *XMM–Newton* and *NuSTAR* spectra, and then use WEBPIMMS http://heasarc.gsfc.nasa.gov/Tools/w3pimms.html to convert this to an equivalent *Swift*–XRT count rate.

Table 2. Best-fitting parameters for the *XMM–Newton* outburst observations when fitted with simple phenomenological continuum models. The first two columns report the *XMM–Newton* OBSID and the source state (see Section 3). The following three columns report the best-fitting neutral column density and spectral index parameters and the χ^2/dof obtained for an absorbed power-law model (`phabs*power`). The following three columns report the neutral column density, the disc blackbody temperature, the minimum χ^2 and the dof obtained for an absorbed disc blackbody model (`phabs*diskbb`). The ninth column shows the χ^2 and the dof obtained for an absorbed disc blackbody model (`phabs*diskbb`), once the Fe K band ($5.5 < E < 8.5\,\mathrm{keV}$) is excluded from the fit. The last column reports the difference in χ^2 between the best-fitting absorbed power-law model minus the best-fitting absorbed disc blackbody model.

XMM–Newton OBSID	State	phabs*power-law N_{H} ($10^{22}\,\mathrm{cm}^{-2}$)	Γ	χ^2/dof	phabs*diskbb N_{H} ($10^{22}\,\mathrm{cm}^{-2}$)	T_{DBB} (keV)	χ^2/dof	χ^2/dof (no Fe K)	$\Delta\chi^2$ PL−BB
0690441801	H	18.9 ± 0.5	1.85 ± 0.05	1347.5/1259	15.6 ± 0.4	3.3 ± 0.1	1372.9/1034		-63.3
0724210501	S	24.1 ± 0.4	3.07 ± 0.04	639.8/332	17.3 ± 0.3	1.95 ± 0.03	425.4/332	202.7/192	223.1
0700980101	S	25.8 ± 0.4	2.99 ± 0.03	908.9/332	19.1 ± 0.3	2.00 ± 0.02	500.6/332	200.9/192	469.5
0724210201	S	25.6 ± 0.3	2.83 ± 0.03	986.7/332	19.2 ± 0.2	2.12 ± 0.02	506.4/332	208.8/192	528.4
0505670101	S	25.8 ± 0.3	2.97 ± 0.03	952.8/332	19.2 ± 0.2	2.00 ± 0.02	570.2/332	198.1/192	388.8
0511000301	S	25.7 ± 1.0	2.96 ± 0.10	374.9/332	19.2 ± 0.7	2.01 ± 0.07	346.6/332	208.0/192	28.5
0504940201	S	25.5 ± 0.7	3.09 ± 0.08	429.0/332	18.6 ± 0.6	1.94 ± 0.05	374.1/332	194.1/192	55.8
0402430401	S	26.3 ± 0.3	2.82 ± 0.03	813.0/332	20.0 ± 0.2	2.11 ± 0.02	499.4/332	193.0/193	349.6
0402430301	S	24.9 ± 0.3	2.76 ± 0.03	965.1/332	18.9 ± 0.2	2.16 ± 0.02	577.1/332	202.6/192	349.5
0402430701	S	25.8 ± 0.4	2.86 ± 0.04	592.0/332	19.4 ± 0.3	2.08 ± 0.03	405.9/332	163.8/192	192.2
0302882601	H	21.8 ± 2.1	1.99 ± 0.20	247.1/246	17.8 ± 1.6	3.04 ± 0.38	254.3/246		-2.5

distance of ~8–20 kpc, AX J1745.6-2901 has a peak luminosity of $L \sim 3$–$30 \times 10^{36}\,\mathrm{erg\,s}^{-1}$ (see Section 4.2), corresponding to several per cent of the Eddington luminosity (for an NS mass of $1.4\,\mathrm{M}_\odot$). The small angle between AX J1745.6-2901 and Sgr A⋆, and the significant increase in surface density of stars and X-ray binaries towards the Galactic Centre (e.g. Muno et al. 2003), makes the Galactic Centre the most probable location. Therefore, we assume a distance to AX J1745.6-2901 of 8 kpc. Such a distance is further supported by observations of the brightest X-ray bursts emitted by AX J1745.6-2901, which reached the Eddington luminosity for an NS at 8 kpc (Maeda et al. 1996, Degenaar & Wijnands 2009). The luminosities computed in this work can be scaled by a factor $(\mathrm{dist}/8\,\mathrm{kpc})^2$, should a more reliable measurement of the distance of AX J1745.6-2901 become available.

It is well known that, at luminosities in the range 1–30 per cent L_{Edd}, NS–LMXBs typically alternate between two distinct states (e.g. van der Klis 2006), with state transitions following a hysteresis pattern in the hardness–intensity diagram (HID; Muñoz-Darias et al. 2013). The X-ray spectra of NS–LMXBs in outburst (see Barret 2001; Lin, Remillard & Homan 2007) are characterized by two main states: (i) a hard state where the 3–10 keV emission is dominated by a power-law component and strong variability (rms up to ~20–40 per cent); (ii) a soft state where the X-ray emission is dominated by a disc blackbody component and there is only weak broad-band variability (rms < 5 per cent). Note that the same levels of rms and spectral properties characterize the hard and soft state in BH X-ray binaries as well (e.g. Muñoz-Darias et al. 2011). NS–LMXBs can also show an additional X-ray emission component, associated with emission from the surface of the NS. Furthermore, the observed spectrum of AX J1745.6-2901 is significantly modified by absorption from a high column density of neutral material (consistent with observations of other Galactic Centre sources).

To determine the state of AX J1745.6-2901 in outburst, we investigated two independent measures: the X-ray variability and the shape of the X-ray continuum. We fitted the spectrum from each *XMM–Newton* OBSID with three different continuum models [all absorbed by a column density of neutral material fitted with the `phabs` model with Anders & Grevesse (1989) abundances and Balucinska-Church & McCkammon (1992) cross-sections]. They

are (i) a multitemperature disc blackbody (`phabs`×`diskbb`); (ii) a single temperature blackbody component (`phabs`×`bbody`) and (iii) a power-law (`phabs`×`powerlaw`) continuum model. We report in Table 2 the χ^2 and best-fitting values for the power-law model and disc blackbody as well as the differences between the χ^2 for the best-fitting power-law model compared to the χ^2 for the best-fitting blackbody model. We find that for each of the observations where AX J1745.6-2901 has a high flux, the thermal (blackbody and disc blackbody) models give a significantly better fit compared to the power-law model. The power-law model is preferred in the two observations at the lowest flux. At the highest fluxes, the best-fitting power-law spectral index indeed assumes very steep values ($\Gamma \sim$ 2.8–3.1) suggesting instead the presence of a thermal component. Despite the blackbody and disc blackbody models well reproducing the shape of the continuum of the high-flux observations, the presence of very significant residuals in the Fe K band makes the fit formally unacceptable (see Table 2). We note that an acceptable fit is obtained once the Fe K band ($5.5 < E < 8.5\,\mathrm{keV}$) is excluded (see column 9 in Table 2).

We also investigated the X-ray variability of AX J1745.6-2901. We produced light curves in the 3–10 keV energy band[4] from the *XMM–Newton* EPIC-pn data, with 73 ms time resolution,[5] and cleaned of time intervals associated with dips and bursts (using the same criteria and thresholds used in Section 2.1 and Table 1). These light curves were used to compute the power spectral density (PSD) function of each OBSID and to derive an estimate of the high-frequency (i.e. 0.1–7 Hz) fractional rms. However, since the detected EPIC-pn count rate is typically fairly low (i.e. between 0.8 and 7 ct s^{-1}), the PSDs are dominated by counting noise and do not permit a reliable measurement of the intrinsic source variability.

---

[4] We consider only the hard X-ray band because, due to the high column density of neutral material towards AX J1745.6-2901, only a small fraction of $E < 3\,\mathrm{keV}$ source photons reach us (see e.g. Maeda et al. 1996; Degenaar & Wijnands 2010a; or Fig. 5).

[5] This is the finest time resolution available for the PrimeFullWindow observing mode.
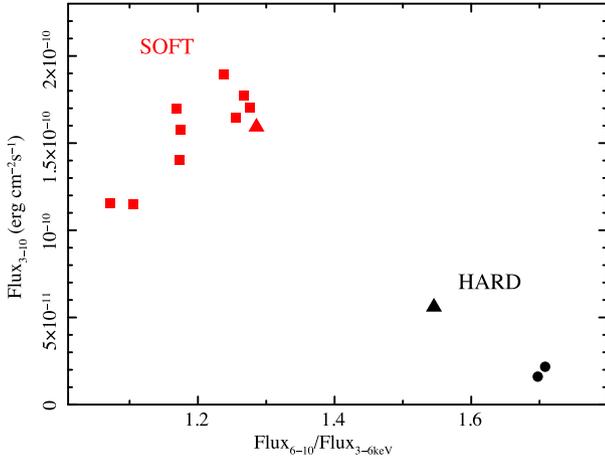
Figure 2. HID for AX J1745.6-2901. Red squares and black circles indicate soft and hard-state *XMM–Newton* observations, respectively. Soft-state observations are fitted best by a simple blackbody or disc blackbody model, while hard states are fitted best by a power-law emission model. Triangles show the hardest and softest *NuSTAR* observations used to constrain the source SED (to compute proper ionized absorber models, Section 5.2).

Finally, we identify the position of each observation of AX J1745.6-2901 in the HID (see Fig. 2), which is often used to determine the source state (Fender, Belloni & Gallo 2004; Belloni, Motta & Muñoz-Darias 2011; Muñoz-Darias et al. 2013). The hardness ratio is defined here as the ratio between the observed fluxes in the 6–10 and the 3–6 keV bands. As expected, thermal emission-dominated observations have a markedly smaller hardness ratio compared to power-law-dominated ones. Note that the observed hardness ratio indicates a real variation of the SED (e.g. it is not due to a variation of the neutral absorber; see Section 4.1). We therefore denote the thermal emission softer observations as 'soft state' and the power-law-dominated harder observations as 'hard state'.

4 PHENOMENOLOGICAL MODELS

In what follows (guided by the results presented in Section 3), we consider only an absorbed power-law spectral model for the hard-state observations, and either an absorbed disc blackbody or an absorbed single blackbody component for the soft-state observations (see Table 2).

4.1 Neutral absorbing material

Fig. 3 shows the best-fitting column density of neutral material during the soft- and hard-state observations. These measurements are consistent with a constant column density, despite the very large variation in source flux and spectral shape. This suggests that, despite AX J1745.6-2901 being a dipping source, the observed column density of neutral material is most probably attributable to absorption along the line of sight, i.e. physically unrelated to AX J1745.6-2901. In fact, the observed column density is within a factor of 2 of the column densities measured towards two other nearby Galactic Centre sources: Sgr A* and SGR J1745-2900, $N_H = 1.1$ and 1.7×10^{23} cm^{-2}, respectively (Baganoff et al. 2003; Trap et al. 2011; Nowak et al. 2012; Rea et al. 2013). This high column density of neutral material supports the hypothesis that AX J1745.6-2901 is located either at or behind the Galactic Centre.
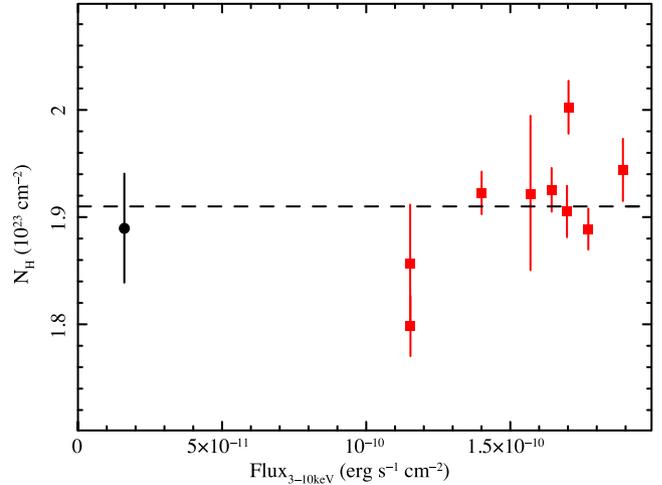

Figure 3. Column density (in units of 10^{23} cm^{-2}) of neutral material as a function of the observed 3–10 keV flux. Red squares and black circles show soft- and hard-state observations, respectively.

4.2 Thermal emission in the soft state

The upper panel of Fig. 4 shows the best-fitting temperature and luminosity for the soft-state spectra fitted with a simple blackbody. During these observations, AX J1745.6-2901 is observed at a luminosity between $L \sim 2$–4×10^{36} erg s^{-1}. Given the high inclination of the system, it is probable that the intrinsic disc luminosity is much higher. For example, simple geometrical considerations (not taking into account relativistic effects) suggest that for AX J1745.6-2901's inclination angle of $\theta \sim 80°$, the intrinsic disc luminosity should be a factor of $\cos(\theta \sim 80°)^{-1} \sim 3$ higher than the observed luminosity.[6] Therefore, the intrinsic disc luminosity of AX J1745.6-2901 corresponds to $\sim$4–10 per cent Eddington (versus $\sim$1.2–2.6 per cent Eddington for the uncorrected luminosity). This places AX J1745.6-2901 in the typical luminosity range observed in 'atoll' sources (Gladstone, Done & Gierliński 2007; Muñoz-Darias et al. 2013). AX J1745.6-2901 would be characterized by even higher luminosities if it is in fact located far behind the Galactic Centre.

The upper panel of Fig. 4 shows a clear trend of larger luminosities with increasing blackbody temperatures. Blackbody temperature and luminosities are well correlated with a Spearman correlation coefficient of 0.78 (with an associated null hypothesis probability of 1.3×10^{-2} corresponding to a confidence level of 98.7 per cent).[7] The line in Fig. 4 shows the relation, $L_{BB} \propto kT_{BB}^4$ that is expected when the thermally emitting region varies in temperature but keeps a constant area. This simple relation reproduces the observed

---

[6] The inclination of AX J1745.6-2901 was proposed to be $\sim$70° by Maeda et al. (1996). However, this value is a lower limit since (i) it assumes a 1 M$_\odot$ main-sequence companion and (ii) the eclipses should be grazing. On the other hand, an inclination $\gtrsim$85° is not expected since the system does not show the typical properties of accretion disc corona sources (e.g. White & Holt 1982). Since the companion stars in LMXBs are typically evolved (and thus less massive than expected for a main-sequence star), and this source displays relatively deep eclipses, we adopt an inclination angle of 80°. In any case, we note that our results are not significantly dependent on small variations of this orbital parameter.

[7] See appendix A of Bianchi et al. (2009; see also Ponti et al. 2012b) for details on this procedure, which takes into account errors on the Y variable.
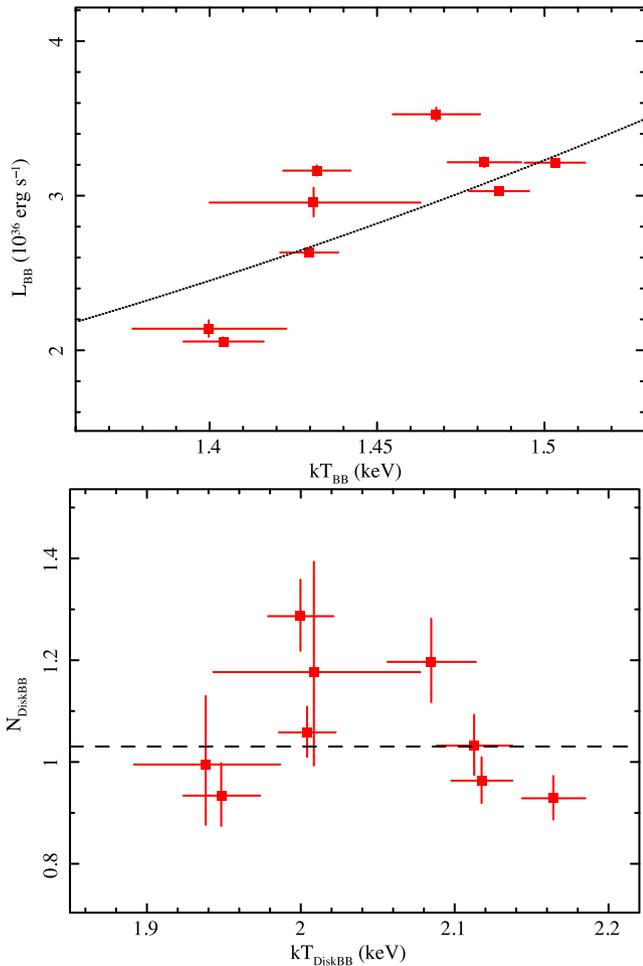
Figure 4. Top panel: observed disc luminosities (in units of 10^{36} erg s^1) versus disc temperature (in keV) obtained from fits with the `phabs×bbody` model. The dotted line shows the best-fitting relation ($L_{BB} \propto kT_{BB}^4$). Bottom panel: multitemperature disc blackbody normalization as a function of disc temperature.

trend; however, significant intrinsic scatter is present. This scatter might be produced by the emission from the boundary layer. In addition, the $L_{BB} \propto kT_{BB}^4$ trend is supported by the results of spectral fits using a disc blackbody component (see the lower panel of Fig. 4), which, to first approximation, are consistent with a disc having constant normalization and an inner radius $R_{in} \sim 12$ km (assuming a disc inclination of 80° and a colour to effective temperature ratio $k = 2$; Shimura & Takahara 1995; Kubota et al. 1998).

4.3 Soft and hard state comparison

Fig. 5 shows the combinedtime-averaged spectra of all the soft- and all the hard-state *XMM–Newton* observations, and their residuals with respect to an absorbed blackbody model (soft state) and to an absorbed power-law model (hard state).

Systematic negative residuals at the energies of the Fe xxv and Fe xxvi transitions are clearly visible in the time-averaged soft-state spectrum. These absorption features are also visible, albeit at lower signal-to-noise ratio, in the spectra from individual soft-state observations. The combined soft-state spectrum shows very significant residuals at the energies of the Fe xxv Kα ($E = 6.697$ keV) and Fe xxvi Kα ($E = 6.966$ keV), as well as Fe xxv Kβ ($E = 7.880$ keV)

and Fe xxvi Kβ ($E = 8.268$ keV) lines, with a possible contribution from Ni xxvii Kα and Fe xxv Kγ lines. Similar absorption lines were also observed by Hyodo et al. (2009) in a single *Suzaku* observation. These features are therefore most probably produced by absorption from photoionized gas. In contrast, no significant narrow negative residuals are visible in the time-averaged hard-state spectrum, nor in the spectra from the individual hard-state observations, with upper limits to the absolute value of the line equivalent width as stringent as ∼5–15 eV.

This one-to-one correlation of wind absorption with accretion state appears similar to that seen in the other well-monitored NS, EXO 0748-676 (Ponti et al. 2014) and in Galactic BH binaries (Miller et al. 2008, 2012; Neilsen & Lee 2009; Ponti et al. 2012).

4.4 Fe xxv and Fe xxvi absorption line inter-observation variability

In order to examine in more detail the variability of these absorption lines, we fit the spectrum from each soft-state observation with an absorbed single blackbody model plus two narrow absorption lines: (`phabs×(gaus+gaus+bbody)`). Such lines have been observed in most high-inclination LMXBs and they are typically unresolved at the EPIC-pn CCD resolution (Díaz-Trigo et al. 2006). However, grating observations of such features reveal typical widths of ∼ few 10^2 km s^{-1} for these lines (Miller et al. 2008; Kallman et al. 2009). Therefore, at first, we fix the line widths of the Fe xxv and Fe xxvi absorption lines to 5 eV. For the measurement of absorption lines, we consider only the seven soft-state *XMM–Newton* observations having clean exposure times longer than 5 ks (see Table 3). The addition of the two narrow absorption lines significantly improves the fit (compared to a simple absorbed blackbody model) from $\chi^2 = 3333$ for 2324 dof to $\chi^2 = 2578$ for 2296 dof. Clear residuals are still observed at energies corresponding to the Fe xxv Kβ and Fe xxvi Kβ lines. Addition of these two ionized narrow (with width fixed to 5 eV) Fe Kβ absorption lines to the spectral model significantly improved the fit to $\chi^2 = 2334$ for 2270 dof. The best-fitting parameters of these fits are reported in Table 3. To test whether or not these lines appear resolved, we then tie the width of all the lines to a single value that is left free to vary. We obtain a best-fitting energy of $\sigma = 0.035 \pm 0.015$ keV, corresponding to $v \sim 1400 \pm 500$ km s^{-1}. However, we observe only a small improvement of the fit ($\chi^2 = 2328$ for 2269 dof, with associated *F*-test probability 0.018), suggesting that these absorption lines are not (or are barely) resolved. Therefore, in the analysis that follows we keep the line widths fixed to 5 eV.

4.4.1 Fe K line energies

The left-hand panel of Fig. 6 shows the best-fitting energies of the Fe xxv Kα and Fe xxvi Kα absorption features and the expected energies of the resonance Fe xxvi Kα and Fe xxv Kα lines and inter-combination Fe xxv Kα transitions (see also Table 3). No significant blue- or redshift is observed. However, due to the finite energy resolution and the uncertainty on the energy-scale calibration of the EPIC-pn camera, only outflows with $v_{out} \gg 10^3$ km s^{-1} would be detected. Higher energy resolution observations (together with better energy-scale calibration) are thus required to measure outflows that are typically observed in Galactic BHs ($v_{out} \sim 10^2$–10^3 km s^{-1}). Note that the Fe xxv and Fe xxvi Kβ absorption features are observed at the expected energies of these transitions (see Table 3).
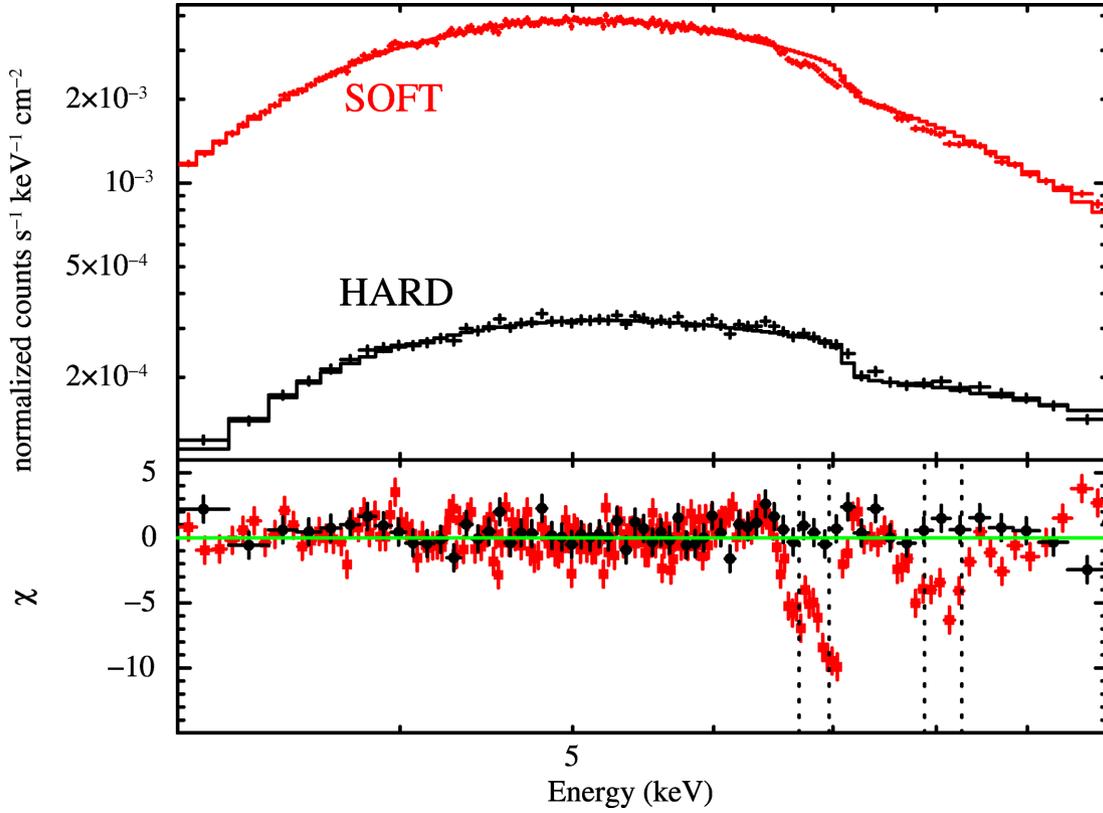
Figure 5. The combined spectrum from all soft-state *XMM–Newton* observations is shown with red squares. The combined spectrum for hard-state observations is shown with black circles. The continuum is fitted with an absorbed blackbody (soft state) and power-law (hard state), see Section 4.2. Significant absorption features at the energies of the Fe xxv Kα and Fe xxvi Kα, as well as Fe xxv Kβ and Fe xxvi Kβ (indicated by the dotted lines) are clearly visible in the combined spectrum for the soft-state observations. There are no obvious residuals due to ionized narrow absorption lines in the combined spectrum for the hard-state observations.

Table 3. Best-fitting model parameters obtained for the high statistics *XMM–Newton* soft-state spectra when fitting with the absorbed blackbody plus four Gaussian line model `phabs*bbody*(gauss+gauss+gauss+gauss)`. The first two columns report the *XMM–Newton* OBSID and the state of the source. The following eight columns show the best-fitting energy and equivalent width (or upper limit) for the Fe xxv Kα, Fe xxvi Kα, Fe xxv Kβ and Fe xxvi Kβ lines, respectively. All lines are significantly detected in each high-quality soft-state spectrum. Only upper limits on the equivalent widths are observed during the hard-state observations (only the longer hard-state *XMM–Newton* observation is reported here). The last column reports the best-fitting χ^2/dof for the absorbed blackbody model plus four Gaussians. †The hard-state spectrum is fitted with an absorbed power-law model.

XMM–Newton		phabs*bbody*(gaus+gaus+gaus+gaus)								
OBSID		Fe xxv Kα		Fe xxvi Kα		Fe xxv Kβ		Fe xxvi Kβ		
		E (keV)	EW (eV)	E (keV)	EW (eV)	E (keV)	EW (eV)	E (keV)	EW (eV)	χ^2/dof
0690441801	H†		> -7		> -13					
0724210501	S	6.69 ± 0.05	-17.6 ± 7.5	6.94 ± 0.02	-33.3 ± 8.1	7.88 ± 0.05	-37.9 ± 10.8	8.17 ± 0.02	-16.2 ± 13.0	319.1/324
0700980101	S	6.73 ± 0.04	-16.9 ± 6.0	6.96 ± 0.03	-31.0 ± 6.7	7.93 ± 0.04	-16.5 ± 9.0	8.22 ± 0.02	-23.2 ± 9.8	327.2/324
0724210201	S	6.75 ± 0.04	-13.5 ± 4.9	6.98 ± 0.03	-20.1 ± 5.5	7.88 ± 0.04	-17.2 ± 7.5	8.24 ± 0.03	-17.5 ± 8.2	379.8/324
0505670101	S	6.64 ± 0.02	-28.7 ± 4.9	6.95 ± 0.02	-32.4 ± 5.6	7.83 ± 0.02	-25.2 ± 7.8	8.17 ± 0.02	-34.0 ± 8.7	348.3/324
0402430401	S	6.68 ± 0.02	-33.3 ± 5.8	6.99 ± 0.03	-23.2 ± 6.9	7.87 ± 0.02	-26.3 ± 9.2	8.17 ± 0.03	-24.8 ± 10.3	321.8/324
0402430301	S	6.65 ± 0.02	-26.9 ± 4.8	6.94 ± 0.02	-35.9 ± 5.2	7.78 ± 0.02	-11.6 ± 7.1	8.17 ± 0.02	-25.2 ± 8.1	339.3/324
0402430701	S	6.68 ± 0.04	-22.8 ± 7.1	6.99 ± 0.02	-39.1 ± 8.0	7.80 ± 0.04	-32.2 ± 10.1	8.19 ± 0.02	-27.3 ± 12.7	287.4/324

4.4.2 Fe K line equivalent widths

The middle and right-hand panels of Fig. 6 show the observed equivalent widths of the Fe xxv, Fe xxvi Kα and Kβ absorption lines (see also Table 3). These four absorption lines are all significantly detected in the individual spectrum from each soft-state observation, with average equivalent widths in the range ~ -40 to -15 eV. In contrast, from the single hard-state spectrum, we can only derive

stringent upper limits (see Fig. 6 and Table 3). Within the soft-state observations, we observe no clear trend of increasing or decreasing line equivalent widths with the 8–10 keV flux. Fig. 6 shows that both the Fe xxvi Kα (middle panel) and Kβ (right-hand panel) lines are typically more intense (~ 15–20 per cent) than the corresponding Fe xxv lines. The ratio between the equivalent widths of the Fe xxv and Fe xxvi lines is a sensitive probe of variations in the ionization state of the absorbing highly ionized plasma. The left-hand panel
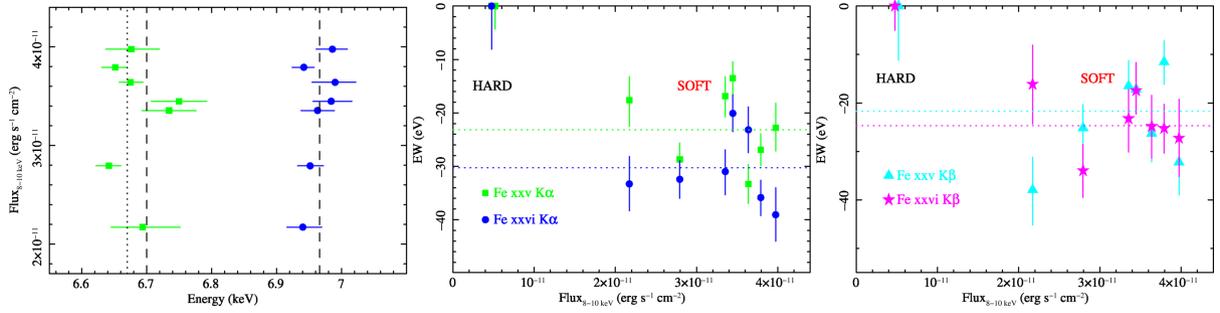
Figure 6. Left-hand panel: best-fitting energies of the Fe xxv and Fe xxvi Kα lines. The vertical lines indicate the energies of the resonance Fe xxvi and Fe xxv lines (dashed) and the inter-combination Fe xxv transition (dotted). Middle panel: equivalent widths of the Fe xxv and Fe xxvi Kα absorption lines (shown in green and blue, respectively) as a function of the 8–10 keV flux. Both lines are significantly detected in each soft-state observations, and stringent upper limits can be placed on the lines during the hard-state observation. Right-hand panel: equivalent widths of the Fe xxv and Fe xxvi Kβ absorption lines (shown in cyan and magenta, respectively) as a function of the 8–10 keV flux. In all three panels, the error bars indicate the one sigma uncertainties (or limits).
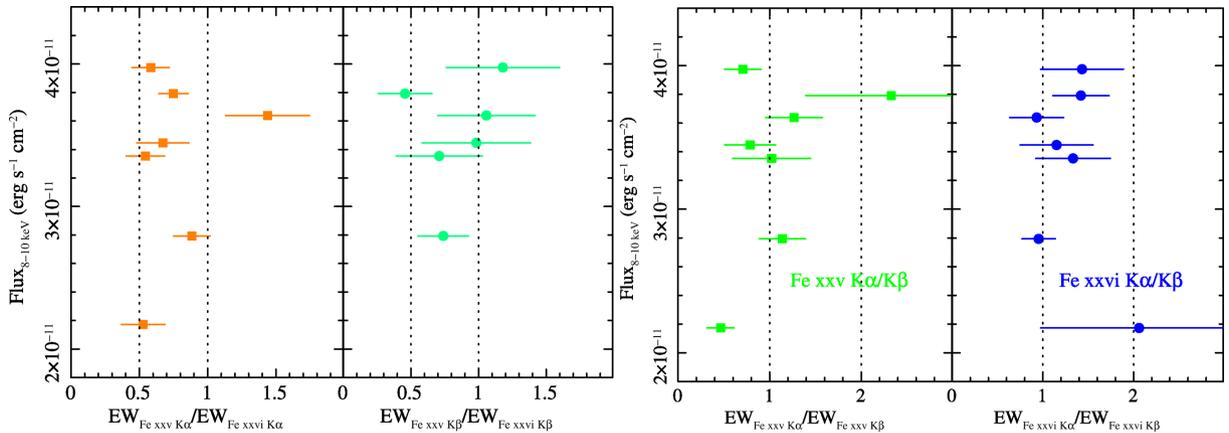
Figure 7. Left-hand panel, left half: ratios of the equivalent width of the Fe xxv Kα line to the equivalent width of the Fe xxvi Kα line as a function of the 8–10 keV flux. Left-hand panel, right half: same for the Fe xxv Kβ and Fe xxvi Kβ lines. Right-hand panel, left half: same for the Fe xxv Kα and Fe xxv Kβ lines. Right-hand panel, right half: same for the Fe xxvi Kα and Fe xxvi Kβ lines. Error bars show the 1σ uncertainties.

of Fig. 7 shows the Fe xxv over Fe xxvi equivalent width ratios for both the Kα and Kβ lines. A small scatter between the different soft-state observations is observed (at least for the Kα transitions), suggesting that despite ionization effects being present,[8] they do not play a major role here. In fact, no clear trend with flux is observed. This is probably due to the significant, but small, variations of the 8–10 keV flux.

We also note that the Kα lines are less than a factor of 2 stronger than the corresponding Kβ lines. In particular, the Fe xxv Kβ lines have equivalent widths comparable to the corresponding Kα lines, for both Fe xxv and Fe xxvi. As shown for the case of NGC 3516 (fig. 4 of Risaliti et al. 2005), these Fe Kα/Fe Kβ ratios suggest high column densities for the absorbing medium ($N_H \gtrsim 10^{23}$ cm^{-2}) and high turbulent velocities of the order of $v_{turb} \sim 500$–1000 km s^{-1}. Note that the Fe xxv and Fe xxvi Kβ lines could have a contribution from Ni xxvii Kα and Fe xxv Kγ, respectively (see e.g. Hyodo et al. 2009). However, these transitions have oscillator strengths significantly lower than the nearby Fe Kβ transitions; therefore, little contribution is expected. Also note that the possible contribution due to these lines has been considered by Risaliti et al. (2005).

---

[8] Given the high densities expected within such ionized absorbers in binaries, the recombination time is expected to be much shorter than the typical time intervals between the *XMM–Newton* observations.

5 PHOTOIONIZATION MODELS

To obtain realistic measurements of the ionization state and column density of the absorbing ionized plasma, we now fit the observed spectra with realistic photoionization models. Therefore, we substitute the multi-Gaussian components with a single photoionized component. In such an analysis, the relative strengths of the various absorption features are tied together in a physical manner.

5.1 Fits with the *zxipcf* model

For an initial, approximate description of the ionized absorption (IA), we use the `zxipcf` model, assuming that the obscuring plasma is totally covering the X-ray source: `phabs×zxipcf×(bbody)`. This component reproduces the absorption from photoionized gas illuminated by a power-law source with spectral index $\Gamma = 2.2$ and is calculated assuming a microturbulent velocity of 200 km s^{-1} (Miller et al. 2007; Reeves et al. 2008). The addition of such a component drastically improves the fit ($\Delta\chi^2 = 789.5$ for 14 new parameters) compared to the fit with a simple absorbed blackbody model (see Fig. 8). We find best-fitting column densities for the photoionized plasma in the range $N_H \sim 1$–4×10^{23} cm^{-2} (see the upper panel of Fig. 9) and best-fitting ionization parameters $\log(\xi/1\,\mathrm{erg\,cm\,s}^{-1}) = 3.9$–4.4 (lower panel of Fig. 9). The column density of the ionized absorber is consistent with being constant between the different soft-state observations (Fig. 9). Due to the
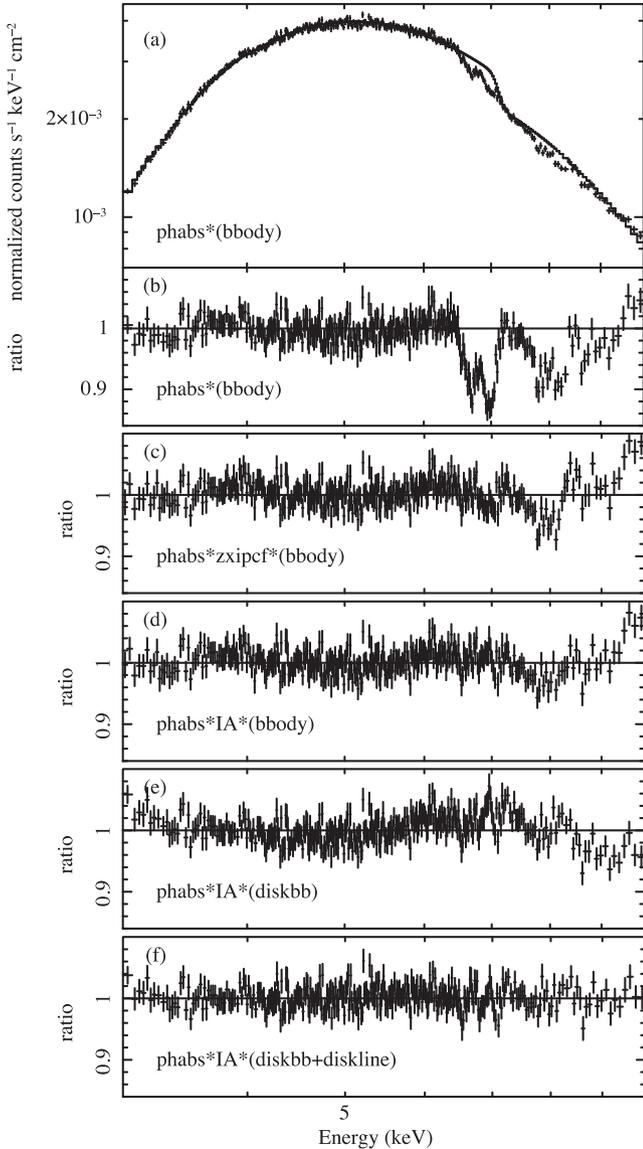
Figure 8. Panel (a): combined soft-state spectra and best-fitting model (`phabs*IA*(bbody)`), once the ionized absorption (IA) component is removed. Panel (b): same as panel (a), but showing the data to model ratio. Panel (c): data to model ratio of the combined soft-state spectra with the `zxipcf` component to fit the IA. Panels (d)–(f): data to model ratio of the combined soft-state spectra with the models: `phabs*IA*(bbody)`, `phabs*IA*(diskbb)` and `phabs*IA*(diskbb+diskline)`, respectively.

high interstellar extinction towards AX J1745.6-2901, we cannot detect additional absorption lines (besides Fe K), and hence we can place only loose constraints on the plasma ionization parameter. Furthermore, the soft-state *XMM–Newton* observations span only a small range ($\sim$ a factor of 2) in luminosity. Therefore, we cannot discriminate between a constant ionization parameter (dotted lines in Fig. 9) and a scenario where the ionization parameter varies linearly with the source luminosity (as expected in the oversimplified case of a constant SED; see the dashed line in Fig. 9).

As a general comment, we note that the Fe XXV and Fe XXVI Kα and Kβ lines are typically well reproduced by the `zxipcf` component, suggesting that these lines are indeed produced by photoionized absorbing material. However, we note significant residuals in several
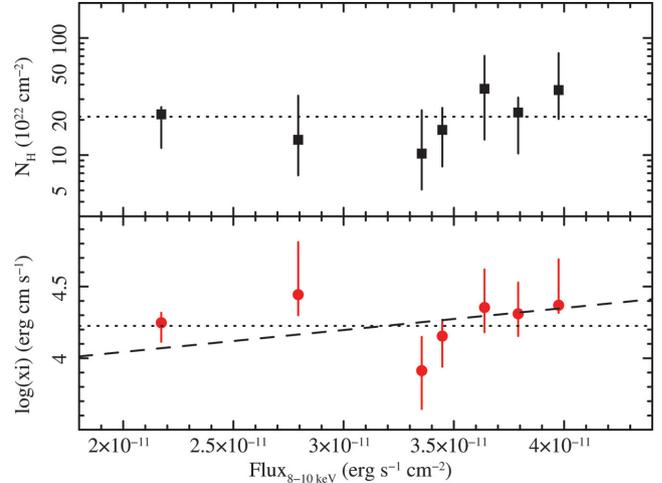
Figure 9. Best-fitting column density (N_{H}, upper panel) and ionization parameter (ξ, lower panel) of the photoionized plasma, as measured using the `zxipcf` spectral model, as a function of the observed 8–10 keV flux. No significant variation is observed in either of the two parameters (the dotted lines show a model with constant N_{H} and ξ). The dashed line shows the best-fitting linear relation between ionization parameter and source luminosity.

of the individual soft-state spectra. This might be related to the small microturbulent velocity used to compute the `zxipcf` table, compared to the high values suggested by the Fe Kα/Fe Kβ line ratios. Indeed, the earlier modelling with independent Gaussian absorption lines resulted in significantly better fits, suggesting that the `zxipcf` component cannot fully reproduce all the details of the observed IA (see Fig. 8).

5.2 Characteristic soft and hard-state SEDs

To compute a physically consistent photoionization model for the Fe K absorption lines, the determination of the source flux and spectral shape in the $\sim$7 to $\sim$10–20 keV band is of primary importance (see the blue-shaded band in Fig. 10). Photons below 7.1 keV cannot ionize the Fe K shell; therefore, they cannot produce either Fe XXV or Fe XXVI absorption lines. However, the physical properties of the ionized absorber (e.g. the plasma temperature) do also depend, albeit weakly, on lower and higher energy photons. To determine the extension of the source emission above $\sim$10 keV, we fit the hardest and softest *NuSTAR* observations of the 2013 campaign to observe Sgr A* (Hailey et al. in preparation). We fit the *NuSTAR* spectra over the 3–79 keV energy band (see the pink band in Fig. 3) with an absorbed disc blackbody model providing the seed photons that are Comptonized and generate a power-law component (`phabs×simpl×diskbb`; Steiner et al. 2009). This allows us to constrain the emission from AX J1745.6-2901 in the full X-ray band. As typical for the soft state (Lin et al. 2007; Plant et al. 2014a,b), the multitemperature disc blackbody emission is well constrained and a very weak and steep power-law component is observed (see Hailey et al. in preparation for more details). A colder disc blackbody emission component is expected to be present during the hard state. Unfortunately, due to the significant Galactic absorption towards AX J1745.6-2901, our data are not sensitive to the disc emission during the hard state. We, therefore assume a fixed temperature of $T_{\mathrm{disc}} = 0.3$ keV (e.g. Plant et al. 2014a,b). We also check that the derived ratio between fluxes of the disc and power-law components is within the typical range observed during the soft and hard states (Remillard & McClintock 2006; Lin et al. 2007).
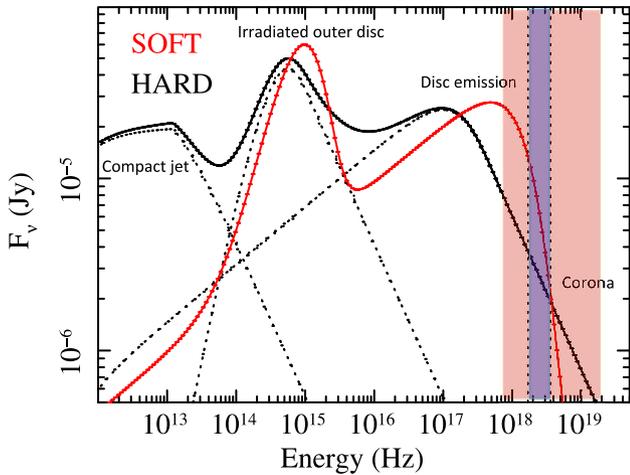
Figure 10. Models for the typical intrinsic SED of AX J1745.6-2901 during the soft (red line) and hard states (black line). The effects of intervening neutral absorption are removed for clarity. The key ingredients described in Section 5.2 to produce the source SED are labelled. The shaded light grey-colour region indicates the energy band over which the SED is constrained by the *NuSTAR* observations ($E = 3$–79 keV). The black region highlights the energy band ($E = 7$–15 keV) just above the Fe K edge, most critical for producing Fe K emission lines.
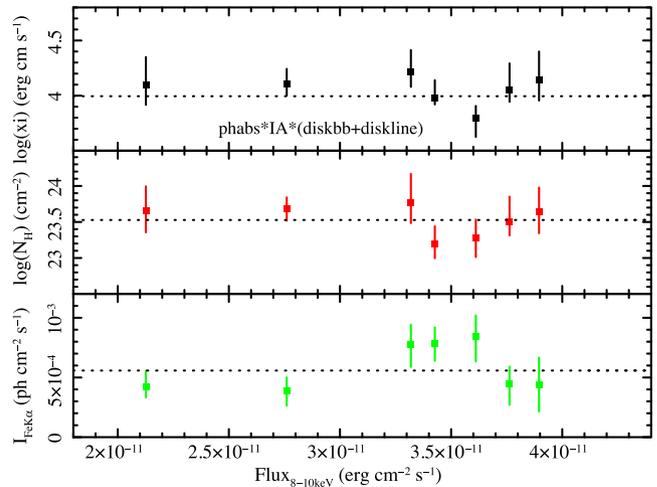

Figure 11. Best-fitting parameter values obtained when fitting the seven high quality soft-state spectra with the model: `phabs*IA*(diskbb+diskline)`, as a function of the 8–10 keV flux. Top panel: logarithm of the ionization state of the ionized absorber. Middle panel: logarithm of the column density of the ionized absorber. Lower panel: intensity of the broad Fe Kα emission line.

Optical and infrared observations of accreting BHs and NS in the soft and hard states show evidence for irradiation of the outer disc (Hynes et al. 2002; Migliari et al. 2010). To model this, we added a thermal (blackbody) component with temperature $T_{\rm BB-S} = 15\,000$ K and $T_{\rm BB-H} = 7000$ K for the soft and hard state, respectively (Hynes et al. 2002). Finally, at radio-to-infrared frequencies, we added a contribution from a compact jet, which is only observed in the hard state (Migliari et al. 2010). The soft and hard-state SED are displayed with red and black lines in Fig. 10, respectively.

5.3 Self-consistent photoionized models

We prepared two ad hoc tables (denoted IA$_{\rm soft}$ and IA$_{\rm hard}$) produced with the photoionization code CLOUDY c13.00 (last described in Ferland et al. 2013). The model ingredients are (1) the soft and hard SEDs presented in Section 5.2; (2) constant electron density $n_e = 10^{12}$ cm^{-3}; (3) ionization parameter in the range $\log(\xi/1\,{\rm erg\,cm\,s}^{-1}) = 3.0$: 5.0; (4) intervening column density in the range $\log(N_H/1\,{\rm cm}^{-2}) = 23.0$: 24.5; (5) turbulence velocity $v_{\rm turb} = 500$: 1000 km s^{-1}; (6) chemical abundances as in table 7.1 of CLOUDY documentation.

We first fit the high-quality soft-state spectra with a model consisting of simple blackbody emission absorbed by both neutral material and by the soft-state photoionized plasma model[9] (model: `phabs*IA`$_{\rm soft}$`*bbody`). To highlight the effect of the ionized absorber, panel (a) of Fig. 8 shows the data and best fit obtained with such a model, once the ionized absorber component has been removed. In the same way, panel (b) of Fig. 8 shows the data-to-model ratio. We show for comparison (panel c) a model consisting of sim-

ple blackbody emission absorbed by both neutral material and by the `zxipcf` component (model: `phabs*zxipcf*bbody`).

Adopting the self-consistent absorber model from CLOUDY (panel d) significantly improves the fit ($\chi^2 = 2458.7$ for 2310 dof) compared to using the `zxipcf` absorber (compared to $\chi^2 = 2543.3$ for 2310 dof). In particular, the fit is improved at the energy ranges corresponding to the Fe Kα and Kβ transitions; strong residuals are no longer present at these energies. However, the fit is still statistically unacceptable (null hypothesis probability *p*-value = 0.016) because significant residuals are still present in the 6–7.5 keV range, as well as an excess of emission above ~9 keV. In Section 4.2, we observed a scaling of the thermal blackbody temperature with luminosity, suggesting an accretion disc origin for this emission, we therefore also attempt to model the continuum by replacing the simple blackbody component with a multitemperature disc blackbody component. We obtain a significantly worse fit (see panel d of Fig. 8) with this model (`phabs*IA*diskbb`; $\chi^2 = 2589.7$ for 2310 dof) and observe strong positive residuals in the range ~5.5–8 keV (panel e of Fig. 8). Note that the disc blackbody model replaces the previous excess above ~9 keV with a slight deficit. To check if the ~5.5–8 keV excess might be produced by a broad Fe Kα line, we add a `diskline` (Fabian et al. 1989) component to the model, representing the emission from a line reflected by an accretion disc (panel f of Fig. 8). We assume the line energy to be $E_{\rm line} = 6.4$ keV (the expected energy from neutral iron), the inner and outer disc radii to be $r_{\rm in} = 6\,r_g$, $r_{\rm out} = 500\,r_g$ and a disc inclination of $i = 80°$ (the disc inner radius is assumed to be $r_{\rm in} = 6\,r_g \sim 12$ km as measured in Section 4.2). We assume the same disc power-law emissivity index (controlling the radial dependence of the emissivity) for all soft-state spectra and obtain a best-fitting value of $\beta = -2.4$. The addition of the `diskline` component significantly improves the fit ($\chi^2 = 2309.6$ for 2301 dof; see Fig. 8). This model now provides a completely statistically acceptable description of the data (*p*-value = 0.45). The broad Fe Kα line component is significantly detected (see Fig. 11) within each *XMM–Newton* observation, with an equivalent width in the range EW ~ 80–200 eV.

---

[9] We fitted the photoionized plasma component with the IA model fixing the turbulent velocity either to $v_{\rm turb} = 500$ or $=1000$ km s^{-1}. Consistent results are obtained. However, assuming $v_{\rm turb} = 500$ km s^{-1} leads to a slightly better fit. For this reason we, hereinafter, assume such turbulent velocity for the ionized plasma.

We note that the best-fitting parameters of the IA component (N_H, ξ) do not vary significantly if the continuum is modelled with either a blackbody or a disc blackbody component, and are also independent of whether the broad iron line is added to or excluded from the fit. The top and middle panels of Fig. 11 show the best-fitting column density and ionization parameter of the ionized absorber model.

Fig. 11 shows that, as previously observed when fitting the absorption features with simple Gaussians or the `zxipcf` model, the ionization level and column density parameters of the CLOUDY ionized absorber model are consistent with being constant during all the soft-state observations. No clear trends with luminosity are observed.

5.4 Does the wind disappear in the hard state because of ionization effects?

As shown in Section 10, the SED of AX J1745.6-2901 changes dramatically between the soft- and the hard state. It is expected that, even if exactly the same absorbing material is present in both states, the variation of the source SED will change the ionized plasma ionization state. For example, an increase of the source luminosity in the 8–10 keV band is expected to increase (possibly overionizing) the plasma ionization, changing the intensities of the Fe XXV and Fe XXVI absorption lines, and vice versa for a decrease in the source luminosity.

To check if this is indeed the case, we fist compute for each soft-state spectrum, from the best-fitting column density and ionization parameter, the product $n \times R_0^2$ (where n is the number density of the ionized absorbing plasma and R_0 is its distance from the primary source). In fact, a variation of the SED will change the ionization state of the plasma, but it will leave the product $n \times R_0^2$ constant (unless the plasma undergoes a true physical variation). Within the soft-state observations, we observe this product to remain constant, with an average value of $n \times R_0^2 = 4.8 \times 10^{32}$ cm^{-1}. To test if the absorber physically varied during the hard state, we first assume the same observed product also for the hard-state observations. We then derive, given the observed SED, the absorbing plasma ionization parameter for each hard-state observation. In particular, the highest statistics hard-state observation (OBSID: 0690441801) is expected to have an ionization parameter $\log(\xi/1\,\mathrm{erg\,cm\,s^{-1}}) = 3.19$. We then fit this spectrum with the self-consistently IA model (`phabs*IA_hard*diskbb`), imposing the expected ionization parameter and leaving the column density free to vary between the lowest and highest value observed during the soft-state observation. Even for the lowest column density observed during the soft state, the hard-state ionization model predicts, at such ionization state, a very strong Fe XXV Kα line (see Fig. 12). The presence of such a line is excluded by the data (note that the inclusion of the broad disc line component does not change this conclusion). This suggests that ionization effects are not able to explain the observed behaviour and that a true physical variation of the ionized absorber between the different states is required.

6 CONCLUSIONS

The *XMM–Newton* and *Swift* monitoring observations of the central ~15 arcmin of the Milky Way have detected several outbursts from the accreting NS system AX J1745.6-2901, allowing us to measure the spectral evolution during both the soft and hard states. Nine *XMM–Newton* observations caught AX J1745.6-2901 in the soft
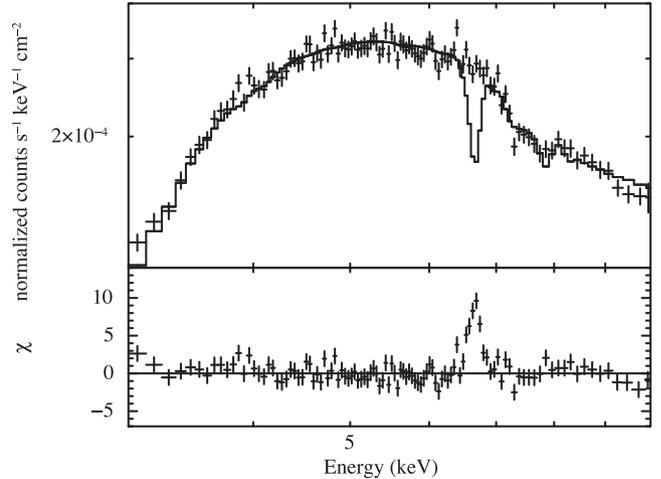

Figure 12. Spectrum of the hard-state observation 0690441801, compared with a model assuming the same ionized plasma observed during the soft state (thus, constant $n \times R_0^2$), allowing only the ionization state to respond to changes in the shape and normalization of the irradiating SED. This model and the data are shown in the top panel, and the residuals to the fit are shown in the bottom panel. The model is clearly excluded.

state and three in the hard state. Our main conclusions/findings can be summarized as follows.

(i) As is commonly observed in NS–LMXB, the persistent emission of AX J1745.6-2901 during the soft state is dominated by a thermal optically thick component, most probably due to multitemperature blackbody emission from the accretion disc, plus blackbody emission from the NS surface. This emission component is observed to vary in temperature with luminosity and to keep its emitting area roughly constant. The hard-state emission (outside of dipping intervals) is well described by a power-law component. The low luminosity of the thermal component is consistent with the high inclination of the system.

(ii) The persistent emission in both the soft and hard state is heavily absorbed by a large column density of neutral material $N_H \simeq 1.9 \times 10^{23}$ cm^{-2}. Such a large column density is within a factor of 2 of that observed towards other Galactic Centre sources along nearby lines of sight, such as Sgr A* and SGR J1745-2900, and is consistent with remaining constant between all *XMM–Newton* observations. This suggests that AX J1745.6-2901 is at (or behind) the Galactic Centre and that most of the obscuring column density is due to the interstellar medium (outside of dipping intervals).

(iii) Highly significant absorption features due to the Fe XXV and Fe XXVI Kα and Kβ lines are detected in the spectra from all nine soft-state observations. The Fe XXV and Fe XXVI Kα lines have typical equivalent widths of EW ~ -20 to 35 eV, very similar to the equivalent widths of the corresponding Kβ lines (EW ~ -15 to 30 eV). No absorption lines are observed in the hard state (very stringent upper limits are measured; EW $\gtrsim -5$ to 10 eV). This wind-Fe K absorber versus state connection is similar to what has been observed in EXO 0748-676, the only accreting NS for which the wind–accretion state connection has been investigated so far (Ponti et al. 2014). Moreover, such behaviour closely resembles what is seen in accreting BH systems, where winds (traced by the same Fe K absorption features) are observed only during the accretion-disc-dominated soft states, and disappear during the hard states characterized by jet emission (Miller et al. 2008, 2012; Neilsen & Lee 2009; Ponti et al. 2012).

(iv) We observe the column density of the ionized material ($N_H \sim 2 \times 10^{23}$ cm^{-2}) to be consistent with being constant within the seven high-statistics soft-state *XMM–Newton* observations. Moreover, we do not observe any trends in the Fe xxvi/Fe xxv Kα and Kβ ratios, with the source 8–10 keV luminosity, between the different soft-state observations. This might be due to the relatively small range of luminosities spanned by the source (less than a factor of 3) and/or be induced by saturation of the lines.

(v) Once the continuum and absorption components are fitted, a broad positive residual remains between $\sim$5.5 and 8 keV. This excess can be reproduced by a standard (EW $\sim$ 80–200 eV) Fe Kα emission line from a standard ($r_{in} = 6~r_g$, $r_{out} = 500~r_g$) accretion disc seen at high inclination. We note that because the system is highly inclined, the Fe Kα line is highly smeared. High signal-to-noise observations are mandatory to reveal the presence of similarly broad emission lines in other high-inclination systems.

ACKNOWLEDGEMENTS

REFERENCES

Anders E., Grevesse N., 1989, Geochim. Cosmochim. Acta, 53, 197
Baganoff F. K. et al., 2003, ApJ, 591, 891
Barret D., 2001, Adv Space Res., 28, 307
Balucinska-Church M., McCammon D., 1992, ApJ, 400, 699
Belloni T. M., Motta S. E., Muñoz-Darias T., 2011, Bull. Astron. Soc. India, 39, 409
Bianchi S., Bonilla N. F., Guainazzi M., Matt G., Ponti G., 2009, A&A, 501, 915
Boirin L., Parmar A. N., 2003, A&A, 407, 1079
Boirin L., Parmar A. N., Barret D., Paltani S., Grindlay J. E., 2004, A&A, 418, 1061
Boirin L., Méndez M., Díaz-Trigo M., Parmar A. N., Kaastra J. S., 2005, A&A, 436, 195
Burrows D. N. et al., 2000, Proc. SPIE, 4140, 64
Cameron D. T., McHardy I., Dwelly T., Breedt E., Uttley P., Lira P., Arevalo P., 2012, MNRAS, 422, 902
Chenevez J. et al., 2006, Astron. Telegram, 756, 1
Clavel M., Terrier R., Goldwurm A., Morris M. R., Ponti G., Soldi S., Trap G., 2013, A&A, 558, A32
Connolly S. D., McHardy I. M., Dwelly T., 2014, MNRAS, 440, 3503

Degenaar N., Wijnands R., 2009, A&A, 495, 547
Degenaar N., Wijnands R., 2010a, A&A, 524, A69
Degenaar N., Wijnands R., Kennea J. A., Gehrels N., 2010b, Astron. Telegram, 2690, 1
Degenaar N., Miller J. M., Kennea J., Gehrels N., Reynolds M. T., Wijnands R., 2013a, ApJ, 769, 155
Degenaar N., Kennea J. A., Wijnands R., Reynolds M. T., Miller J. M., Gehrels N., 2013b, Astron. Telegram, 5226, 1
Degenaar N., Wijnands R., Reynolds M. T., Miller J. M., Kennea J., Gehrels N., 2014a, in Sjouwerman L., Lang C., Ott J., eds, Proc. IAU Symp., 303, The Galactic Center: Feeding and Feedback in a Normal Galactic Nucleus. Cambridge Univ. Press, Cambridge, p. 315
Degenaar N. et al., 2014b, AJ, 792, 109
Díaz-Trigo M., Boirin L., 2013, Acta Polytech., 53, 659
Díaz-Trigo M., Parmar A. N., Boirin L., Méndez M., Kaastra J. S., 2006, A&A, 445, 179
Fabian A. C., Rees M. J., Stella L., White N. E., 1989, MNRAS, 238, 729
Fabian A. C. et al., 2012, MNRAS, 419, 116
Fender R. P., Belloni T. M., Gallo E., 2004, MNRAS, 355, 1105
Ferland G. J. et al., 2013, Rev. Mex. Astron. Astrofis., 49, 137
Gillessen S. et al., 2012, Nature, 481, 51
Gladstone J., Done C., Gierliński M., 2007, MNRAS, 378, 13
Harrison F. A. et al., 2013, ApJ, 770, 103
Heinke C. O., Yusef-Zadeh F., Genzel R., Gillessen S., Menten K. M., Wardle M., 2008, Astron. Telegram, 1513, 1
Hynes R., Jones E., 2008, Astron. Telegram, 1816, 1
Hynes R. I., Haswell C. A., Chaty S., Shrader C. R., Cui W., 2002, MNRAS, 331, 169
Hyodo Y., Ueda Y., Yuasa T., Maeda Y., Makishima K., Koyama K., 2009, PASJ, 61, 99
Kallman T. R., Bautista M. A., Goriely S., Mendoza C., Miller J. M., Palmeri P., Quinet P., Raymond J., 2009, ApJ, 701, 865
Kaspi V. M. et al., 2014, ApJ, 786, 84
Kennea J. A., Skinner G. K., 1996, PASJ, 48, L117
Kennea J. A., Burrows D. N., Campana S., Godet O., Nousek J., Gehrels N., 2006, Astron. Telegram, 753, 1
Kennea J. A. et al., 2013, ApJ, 770, L24
King A. L. et al., 2012, ApJ, 746, L20
Koyama K. et al., 2007, PASJ, 59, 245
Kubota A., Tanaka Y., Makishima K., Ueda Y., Dotani T., Inoue H., Yamaoka K., 1998, PASJ, 50, 667
Lee J. C., Reynolds C. S., Remillard R., Schulz N. S., Blackman E. G., Fabian A. C., 2002, ApJ, 567, 1102
Lewin W. H. G., van Paradijs J., Taam R. E., 1993, Space Sci. Rev., 62, 223
Lin D., Remillard R. A., Homan J., 2007, ApJ, 667, 1073
Maeda Y., Koyama K., Sakano M., Takeshima T., Yamauchi S., 1996, PASJ, 48, 417
Migliari S. et al., 2010, ApJ, 710, 117
Miller J. M. et al., 2006, ApJ, 646, 394
Miller L., Turner T. J., Reeves J. N., George I. M., Kraemer S. B., Wingert B., 2007, A&A, 463, 131
Miller J. M., Raymond J., Reynolds C. S., Fabian A. C., Kallman T. R., Homan J., 2008, ApJ, 680, 1359
Miller J. M., Maitra D., Cackett E. M., Bhattacharyya S., Strohmayer T. E., 2011, ApJ, 7311, 7M
Miller J. M., Pooley G. G., Fabian A. C., Nowak M. A., Reis R. C., Cackett E. M., Pottschmidt K., Wilms J., 2012, ApJ, 757, 11
Mori K. et al., 2013, ApJ, 770, L23
Muno M. P. et al., 2003, ApJ, 589, 225
Muñoz-Darias T., Motta S., Belloni T. M., 2011, MNRAS, 410, 679
Muñoz-Darias T., Coriat M., Plant D. S., Ponti G., Fender R. P., Dunn R. J. H., 2013, MNRAS, 432, 1330M
Neilsen J., Lee J. C., 2009, Nat, 458, 481
Neilsen J., Remillard R. A., Lee J. C., 2011, ApJ, 737, 69
Nowak M. A. et al., 2012, ApJ, 759, 95
Parmar A. N., White N. E., Giommi P., Haberl F., Pedersen H., Mayor M., 1985, IAU circular, 4039, 1
Parmar A. N., White N. E., Giommi P., Gottwald M., 1986, ApJ, 308, 199

Parmar A. N., Oosterbroek T., Boirin L., Lumb D., 2002, A&A, 386, 910

Plant D. S., Fender R. P., Ponti G., Munoz-Darias T., Coriat M., 2014a, A&A, in press

Plant D. S., Fender R. P., Ponti G., Muñoz-Darias T., Coriat M., 2014b, MNRAS, 442, 1767

Ponti G., Terrier R., Goldwurm A., Belanger G., Trap G., 2010, ApJ, 714, 732

Ponti G., Fender R. P., Begelman M. C., Dunn R. J. H., Neilsen J., Coriat M., 2012a, MNRAS, 422, L11

Ponti G., Papadakis I., Bianchi S., Guainazzi M., Matt G., Uttley P., Bonilla N. F., 2012b, A&A, 542, A83

Ponti G., Morris M. R., Terrier R., Goldwurm A., 2013, in Torres D. F., Reimer O., eds, Astrophys. Space Sci. Proc. Vol. 34, Cosmic Rays in Star-Forming Environments. Springer-Verlag, Berlin, p. 331

Ponti G., Muñoz-Darias T., Fender R. P., 2014, MNRAS, 444, 1892P

Porquet D. et al., 2007, Astron. Telegram, 1058, 1

Ratti E. M., Steeghs D. T. H., Jonker P. G., Torres M. A. P., Bassa C. G., Verbunt F., 2012, MNRAS, 420, 75

Rea N. et al., 2013, ApJ, 775, L34

Reeves J., Done C., Pounds K., Terashima Y., Hayashida K., Anabuki N., Uchino M., Turner M., 2008, MNRAS, 385, L108

Remillard R. A., McClintock J. E., 2006, ARA&A, 44, 49

Risaliti G., Bianchi S., Matt G., Baldi A., Elvis M., Fabbiano G., Zezas A., 2005, ApJ, 630, L129

Sakano M., Koyama K., Murakami H., Maeda Y., Yamauchi S., 2002, ApJS, 138, 19

Shimura T., Takahara F., 1995, ApJ, 445, 780

Sidoli L., Oosterbroek T., Parmar A. N., Lumb D., Erd C., 2001, A&A, 379, 540

Steiner J. F., Narayan R., McClintock J. E., Ebisawa K., 2009, PASP, 121, 1279

Trap G. et al., 2011, A&A, 528, A140

Ueda Y., Asai K., Yamaoka K., Dotani T., Inoue H., 2001, ApJ, 556, L87

Ueda Y., Murakami H., Yamaoka K., Dotani T., Ebisawa K., 2004, ApJ, 609, 325

van der Klis M., 2006, Compact Stellar X-ray Sources. Cambridge Univ. Press, Cambridge, p. 39

van Peet J. C. A., Costantini E., Méndez M., Paerels F. B. S., Cottam J., 2009, A&A, 497, 805

Wang Q. D., Gotthelf E. V., Lang C. C., 2002, Nature, 415, 148

White N. E., Holt S. S., 1982, ApJ, 257, 318

Wijnands R. et al., 2007, Astron. Telegram, 1006, 1

Wolff M., Ray P., Wood K., Wijnands R., 2008, Astron. Telegram, 1812, 1

This paper has been typeset from a TEX/LATEX file prepared by the author.